

# SIR epidemics with multiple seeds percolate without outbreaks

Takehisa Hasegawa<sup>1,\*</sup> and Koji Nemoto<sup>2,†</sup>

<sup>1</sup>*Department of Mathematics and Informatics, Ibaraki University, 2-1-1, Bunkyo, Mito, 310-8512, Japan*

<sup>2</sup>*Department of Physics, Hokkaido University, Kita 10 Nishi 8, Kita-ku, Sapporo, 060-0810, Japan*

We study a susceptible-infected-removed (SIR) model with multiple seeds on a random regular graph. Many researchers have studied the epidemic threshold of epidemic models above which a global outbreak can occur, starting from an infinitesimal fraction of seeds. However, there have been few studies on the epidemic models with finite fractions of seeds. The aim of this paper is to clarify what happens on phase transitions in such cases. The SIR model on networks exhibits two percolation transitions. We derive the percolation transition points for the SIR model with multiple seeds to show that as the infection rate increases epidemic clusters generated from each seed percolate before a single seed can induce a global outbreak.

PACS numbers: 89.75.Hc,87.23.Ge,05.70.Fh,64.60.aq

## I. INTRODUCTION

The threat of infectious disease is becoming increasingly conspicuous for the modern society, wherein there is a large amount of international travel all over the world. Understanding how infectious diseases spread in our society is crucial to the development of strategies for disease control. A mathematical model of infectious disease, called the susceptible-infected-removed (SIR) model, was first applied with the assumption of a well-mixed population for the computation of the final numbers of infected and eventually removed (or recovered) individuals [1]. So far, many mathematical models for infectious diseases have been proposed for understanding the spread of epidemics and proposing strategies for disease control [2].

In recent years, many studies have been devoted to epidemic models with a network structure of people [3]. Diseases spread over the networks of physical contacts between individuals, and the structure of real networks [4–7] has crucial effects on this spread. For example, Moreno et al. [8] studied the SIR model on a scale-free network having a degree distribution of  $p_k \propto k^{-\gamma}$  using a degree-based mean-field approach. Their approximation clarified that epidemics can spread over the network for any infection rate if  $\gamma \leq 3$ . In addition, many analytical approaches for epidemic models with network structures, such as the approximation onto a bond percolation problem [9, 10], the edge-based compartment model [11], the effective degree approach [12], and the pair approximation [13, 14], have been proposed and have succeeded in describing epidemic dynamics. Numerical simulations have revealed how epidemics spread in more realistic situations. Also, several strategies for disease control have been proposed on the basis of the knowledge of epidemics on networks, e.g., target immunization [15, 16], acquaintance immunization [16–19], and graph-partitioning immunization [20].

Most previous studies using SIR-type epidemic models have assumed that the fraction of infection seeds is infinitesimally small. In contrast, there have been few studies on epidemic models with finite fractions of seeds. Miller [21] considered the SIR model on networks with large initial conditions to resolve an apparent paradox in works assuming an infinitesimal fraction of seeds. Hu et al. [22] numerically studied how the positions of multiple seeds in a network affect spreading behavior. Ji et al. [23] identified multiple influential spreaders in real networks by ranking nodes in disintegrated networks after random bond removals. What we will discuss here is a more fundamental, but almost overlooked problem: how do epidemic models with finite fractions of seeds undergo phase transitions? For SIR-type epidemics, each infection seed creates an epidemic cluster of infected individuals. Epidemic clusters generated by multiple seeds will have global connectivity in some parameter regions even though each seed may not have the potential to induce a global outbreak there.

In this paper, we consider the SIR model on networks with multiple seeds. In this case, the SIR model exhibits a kind of percolation transitions. An epidemic cluster grows from each multiple seeds as its origin. We regard the clusters so generated as “supernodes” and study the percolation problem of these supernodes. Indeed, we can analytically and numerically obtain the percolation transition point of supernodes to show a gap between this transition point and the epidemic threshold. The existence of this gap indicates that the percolation transition of epidemic clusters

---

\*Electronic address: takehisa.hasegawa.sci@vc.ibaraki.ac.jp

†Electronic address: nemoto@statphys.sci.hokudai.ac.jp

occurs before single seeds can induce a global outbreak. Our result also shows the sensitivity of the seed fraction on percolation transition points, i.e., that a small seed fraction drastically reduces the critical infection rate for the emergence of the infinite epidemic cluster.

## II. MODEL

Let us give a brief review of the SIR model on a given static network. Each node of the network takes one of three states: susceptible, infected, and removed. The system evolves as a continuous-time Markov process. As an initial state configuration, a fraction,  $\rho$ , of the nodes is randomly chosen to be seeds and is initially infected, while other nodes are susceptible. We denote the infection rate by  $\lambda$ . When an infected node is adjacent to a susceptible node, this susceptible node gets infected with probability  $\lambda\Delta t$  within a short time,  $\Delta t$ . Note that this probability is independently given by each of the infected nodes so that the total infection rate at a node is just proportional to the number of infected neighbors. An infected node becomes removed at a rate  $\mu$ , i.e., with probability  $\mu\Delta t$  within a short time  $\Delta t$ , irrespective of the neighbors' states. Without loss of generality, we set  $\mu = 1$  unless otherwise specified. The dynamics stops when no infected nodes exist in the network.

Let us consider the limit  $\rho \rightarrow 0$ . The SIR model exhibits a phase transition at the epidemic threshold  $\lambda = \lambda_c^{\text{SIR}}$  when  $\lambda$  increases from zero. Above  $\lambda_c^{\text{SIR}}$ , a single seed can induce global outbreaks. In a global outbreak, a nonzero fraction of nodes become infected and eventually removed. Below  $\lambda_c^{\text{SIR}}$ , the number of removed nodes is always negligible compared with the total number of nodes. As already mentioned, we have several approaches for obtaining  $\lambda_c^{\text{SIR}}$  (see a recent review [3]); Newman approximated the SIR model on uncorrelated networks by mapping onto a bond percolation problem (which is called the SIR model with transmissibility) [10], and derived  $\lambda_c^{\text{SIR}}$  to be

$$\lambda_c^{\text{SIR}} = \frac{\langle k \rangle}{\langle k^2 \rangle - 2\langle k \rangle}, \quad (1)$$

where  $\langle k \rangle$  and  $\langle k^2 \rangle$  are the first and the second moments of the degree distribution,  $p_k$ , respectively. This result indicates that, for a fat-tailed scale-free network whose degree distribution obeys  $p_k \propto k^{-\gamma}$  with  $\gamma \leq 3$ , a global outbreak starting from an infinitesimal fraction of seeds occurs even for an infinitesimal infection rate. As indicated in [24], mapping onto a bond percolation problem does not give the exact outbreak size or probability, but it does predict exactly the epidemic threshold. Lindquist et al. [12] proposed an effective degree approach for describing the time evolution of the SIR dynamics using numerous ordinary differential equations and derived the same epidemic threshold (1). Miller [11] introduced another approach by means of the edge-based compartment model to enable accurate descriptions of the SIR dynamics accurately with a few rate equations.

We can also describe the phase transition of the present model in terms of percolation. In any final state, each node takes either a susceptible or removed state. We call the connected components of removed nodes and susceptible nodes as the R-components and the S-components, respectively. For the SIR model on networks with  $\rho \gtrsim 0$ , we have two percolation transition points,  $\lambda_{c1}$  and  $\lambda_{c2}$ . When the number of nodes,  $N$ , is much greater than one, the mean fraction of the largest R-component,  $r_{\text{max}}(N) = R_{\text{max}}(N)/N$ , where  $R_{\text{max}}(N)$  is the mean size of the largest R-component, changes from zero to a nonzero value at the former point  $\lambda_{c1}$ . Note that  $\lambda_{c1}$  corresponds with  $\lambda_c^{\text{SIR}}$  in the limit  $\rho \rightarrow 0$  by definition. Percolation analysis of an epidemic cluster starting from a single seed has been used for numerical computations of the epidemic threshold and critical properties [25, 26]. The latter point,  $\lambda_{c2}$ , is on the percolation of the S-component (also called the residual graph [27, 28]) and is usually larger than  $\lambda_{c1}$ . Above  $\lambda_{c2}$ , the network remaining after the removal of the R-components is disintegrated such that the sizes of all remaining components are finite. In other words, the mean fraction of the largest S-component,  $s_{\text{max}}(N) = S_{\text{max}}(N)/N$ , where  $S_{\text{max}}(N)$  is the mean largest S-component size, is zero (nonzero) for  $\lambda > \lambda_{c2}$  ( $\lambda < \lambda_{c2}$ ) when  $N \gg 1$ . Whether the susceptible nodes are globally connected is important because a second epidemic spread may occur on the remaining network [27, 29]. In [27], Newman analyzed this second transition point of the SIR model with transmissibility on uncorrelated networks with  $\rho \rightarrow 0$  to show that the transition point is positive even when  $\gamma \leq 3$ . Valdez et al. [30] proposed a new strategy for suppressing epidemics by regarding this second transition point as a measure of the efficiency of a mitigation or control strategy. If we regard the present model as showing the propagation of an attack against a network, such as a computer virus,  $\lambda_{c2}$  is a measure of the robustness of networks against such attacks [31, 32]. Konno and the authors numerically studied  $\lambda_{c2}$  for correlated networks to show that any positive or negative degree correlation makes networks more robust [32].

To summarize, the system with a given value of  $\rho$  has the following three regions: (i) the S-dominant phase, where  $r_{\text{max}} = 0$  and  $s_{\text{max}} > 0$  for  $\lambda < \lambda_{c1}$ , (ii) the coexisting phase, where  $r_{\text{max}} > 0$  and  $s_{\text{max}} > 0$  for  $\lambda_{c1} < \lambda < \lambda_{c2}$ , and (iii) the R-dominant phase, where  $r_{\text{max}} > 0$  and  $s_{\text{max}} = 0$  for  $\lambda > \lambda_{c2}$ . To investigate in detail about the phase transitions of the SIR model with a finite fraction of seeds, we focus on the  $z$ -regular random regular graph (RRG).

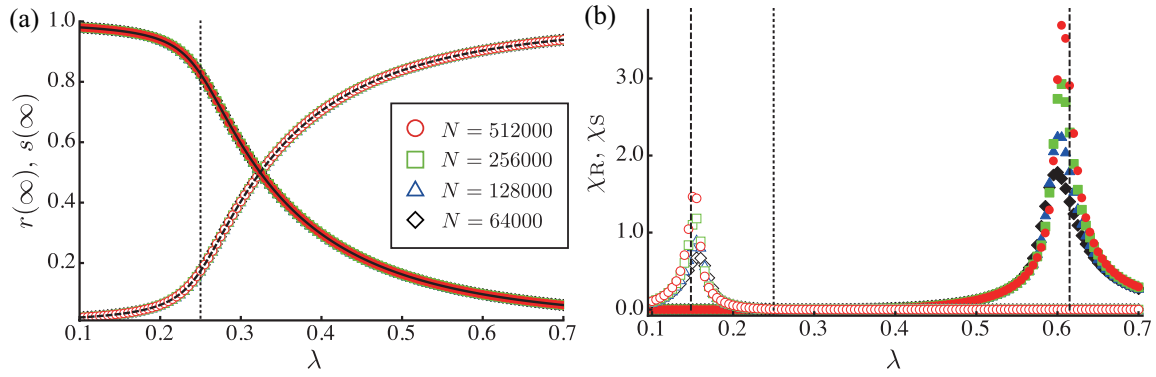


FIG. 1: Numerical results for the SIR model with  $\rho = 0.01$  on the RRG: (a) total densities of the removed nodes  $r$  (open symbols) and of the susceptible nodes  $s$  (filled symbols) and (b) susceptibility of the R-components  $\chi_R$  (open symbols) and of the S-components  $\chi_S$  (filled symbols). The dashed and solid lines in (a) are drawn from the AMEs. In (b), the vertical dotted line represents  $\lambda_c^{\text{SIR}}$ , and the two vertical dashed lines represent  $\lambda_{c1} = 0.148$  and  $\lambda_{c2} = 0.615$ , which will be given in Sec.IV.

Our formulations discussed below are for the RRG, but the extension to networks having degree distribution  $p(k)$  is straightforward.

### III. TOTAL DENSITIES OF SUSCEPTIBLE AND REMOVED NODES

To evaluate the time evolution of the SIR dynamics and the total densities of the susceptible and removed nodes in the final states, we consider the approximate master equations (AMEs) [12, 14].

Let  $s_{l,m}(t)$ ,  $i_{l,m}(t)$ ,  $r_{l,m}(t)$  be the fractions of nodes that are susceptible, infected, and removed, respectively, at time  $t$  and have  $l$  susceptible and  $m$  infected neighbors. The AMEs for the evolution of these variables are as follows:

$$\dot{s}_{l,m} = -\lambda m s_{l,m} + \beta_s^{si} [(l+1)s_{l+1,m-1} - l s_{l,m}] + \beta_s^{ir} [(m+1)s_{l,m+1} - m s_{l,m}], \quad (2)$$

$$\dot{i}_{l,m} = \lambda m s_{l,m} - \mu i_{l,m} + \beta_i^{si} [(l+1)i_{l+1,m-1} - l i_{l,m}] + \beta_i^{ir} [(m+1)i_{l,m+1} - m i_{l,m}], \quad (3)$$

$$\dot{r}_{l,m} = \mu i_{l,m} + \beta_r^{si} [(l+1)r_{l+1,m-1} - l r_{l,m}] + \beta_r^{ir} [(m+1)r_{l,m+1} - m r_{l,m}]. \quad (4)$$

The transition rates of neighboring nodes are approximated as

$$\beta_s^{si} = \lambda \frac{\sum_{l,m} l m s_{l,m}}{\sum_{l,m} l s_{l,m}}, \quad \beta_s^{ir} = \mu \frac{\sum_{l,m} l i_{l,m}}{\sum_{l,m} l i_{l,m}} = \mu, \quad (5)$$

$$\beta_i^{si} = \lambda \frac{\sum_{l,m} m^2 s_{l,m}}{\sum_{l,m} m s_{l,m}}, \quad \beta_i^{ir} = \mu \frac{\sum_{l,m} m i_{l,m}}{\sum_{l,m} m i_{l,m}} = \mu, \quad (6)$$

$$\beta_r^{si} = \lambda \frac{\sum_{l,m} (k-l-m) m s_{l,m}}{\sum_{l,m} (k-l-m) s_{l,m}}, \quad \beta_r^{ir} = \mu, \quad (7)$$

where the summations run over all  $0 \leq l+m \leq k$ . To describe the SIR dynamics with  $\rho > 0$ , we set the initial condition as

$$s_{l,m}(0) = \delta_{k,l+m} (1-\rho) \binom{k}{l} (1-\rho)^l \rho^m, \quad (8)$$

$$i_{l,m}(0) = \delta_{k,l+m} \rho \binom{k}{l} (1-\rho)^l \rho^m, \quad (9)$$

$$r_{l,m}(0) = 0. \quad (10)$$

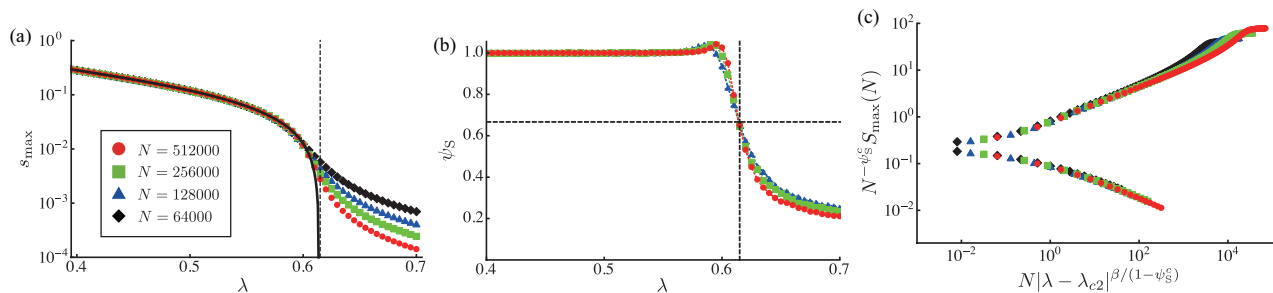


FIG. 2: (a) Fraction of the largest S-component,  $s_{\max}$ , as a function of  $\lambda$ . The points are obtained by Monte-Carlo simulations. The solid line is drawn by evaluating Eq.(17). (b) Numerical results of the fractal exponent of the largest S-component,  $\psi_S$ . Data with several values of  $N$  have a crossing point at  $\lambda_{c2} = 0.615$  and  $\psi_S^c = 2/3$ . (c) Finite size scaling for  $S_{\max}$  around  $\lambda_{c2}$ . Here we set  $\psi_S^c = 2/3$  and  $\beta = 1$ , which means that the transition at  $\lambda_{c2}$  belongs to the mean-field universality class.

By numerical evaluation of the above equations, we obtain the total densities

$$s(t) = \sum_{l,m} s_{l,m}(t), \quad i(t) = \sum_{l,m} i_{l,m}(t), \quad r(t) = \sum_{l,m} r_{l,m}(t), \quad (11)$$

which satisfy the conservation law,

$$s(t) + i(t) + r(t) = 1, \quad (12)$$

at any time  $t$ . Note that all variables other than  $s_{l,0}$  and  $r_{l,0}$  vanish in the limit  $t \rightarrow \infty$ , and therefore  $i(\infty) = 0$ .

To check the accuracy of the AME, we perform Monte-Carlo simulations for the SIR on the RRG with  $z = 6$ . In our simulations, we set  $\mu = 1$  and  $\rho = 0.01$ . The numbers of nodes are  $N = 64000, 128000, 256000, 512000$ . The number of graph realizations is 100, and the number of trials on each graph is 500. Figure 1(a) shows the AME result (line) and the Monte-Carlo result (symbols) of the total densities of susceptible and removed nodes,  $s$  and  $r$ , in the final states. We find that data from the AMEs wholly coincides with those from the Monte-Carlo simulations.

The AMEs do not predict any transition point for  $\rho > 0$  because  $r(\infty) \geq \rho > 0$ , although it is possible to derive the epidemic threshold  $\lambda_c^{\text{SIR}} = \mu/(z-2)$  [12], by considering the limit  $\rho \rightarrow 0$  (see Appendix A). In contrast, the Monte-Carlo simulations suggest that the model actually exhibits phase transitions. In Fig. 1 (b), we plot the R- and S-susceptibilities (which we call the susceptibility by analogy with magnetic susceptibility in spin systems)  $\chi_R$  and  $\chi_S$ . Here,  $\chi_R$  ( $\chi_S$ ) is defined as the mean size of all R-components (all S-components) except the largest one. We find that  $\chi_R$  ( $\chi_S$ ) have peaks at  $\lambda_{c1}$  and  $\lambda_{c2}$ , respectively, implying two phase transitions. Moreover, these points are clearly different from  $\lambda_c^{\text{SIR}}$ . In particular, the gap between  $\lambda_{c1}$  and  $\lambda_c^{\text{SIR}}$  indicates that as the infection rate increases, the epidemic clusters generated from each seed percolate before a single seed can induce a global outbreak. In the next section, we derive these percolation transition points for  $0 < \rho < 1$ .

## IV. PERCOLATION TRANSITIONS OF THE SIR DYNAMICS WITH MULTIPLE SEEDS

### A. derivation of $\lambda_{c2}$

To derive  $\lambda_{c2}$ , we consider the percolation of the S-components. In [27], Newman analyzed the percolation of the S-components using generating functions. His method gives  $\lambda_{c2}$  for the SIR model on uncorrelated networks but assumes a single seed. By combining the AMEs and Newman's method, we obtain  $s_{\max}$  and  $\lambda_{c2}$  for the case with  $0 < \rho < 1$ .

Let us consider the S-components in a typical final state for the SIR model on the infinitely large RRG with  $\rho > 0$ . In the previous section, we already have a probability  $s_{l,0}(\infty)$  that a randomly chosen node is susceptible and has  $l$  susceptible neighbors ( $s_{l,m}(\infty) = 0$  for  $m \neq 0$ ). Using  $s_{l,0}(\infty)$ , we obtain the degree distribution of the S-components as follows:

$$p_l^s = \frac{1}{s} s_{l,0}(\infty), \quad (13)$$

where the denominator  $s = \sum_{l=0}^k s_{l,0}$  is the prior probability of being susceptible. The corresponding generating function,  $F_0^s(x)$ , is given by

$$F_0^s(x) = \sum_{l=0}^k p_l^s x^l. \quad (14)$$

Here we assume that this subnetwork is degree-uncorrelated. Then, the generating function for the excess degree distribution [5] of the S-components is

$$F_1^s(x) = \frac{F_0^{s'}(x)}{F_0^{s'}(1)}, \quad (15)$$

and the mean excess degree is given by  $F_1^{s'}(1)$ . By arguing the emergence of infinitely connected component of this subnetwork (similar to [5]), we easily find that there is an infinite S-component if  $F_1^{s'}(1) > 1$ , and thus, the percolation transition point of the S-component,  $\lambda_{c2}$ , satisfies

$$F_1^{s'}(1) = 1. \quad (16)$$

Following [27], we also have the mean fraction of the largest S-component,  $s_{\max}$ , as

$$s_{\max} = s[1 - F_0^s(v)], \quad (17)$$

where  $v$  is the solution of

$$v = F_1^s(v). \quad (18)$$

We check these estimates using Monte-Carlo simulations. Figure 2(a) shows the order parameter, i.e., the fraction of the largest S-component,  $s_{\max}(N)$ , for RRG with several  $N$ . We find that the numerical results coincide with the analytical line below  $\lambda_{c2}$  and tend to zero with increasing  $N$  above  $\lambda_{c2}$ . To numerically obtain the transition point,  $\lambda_{c2}$ , we introduce the fractal exponent [33]. The fractal exponent of the largest S-component is defined and approximated as

$$\psi_S = \frac{d \ln S_{\max}(N)}{d \ln N} \approx \frac{\ln S_{\max}(N) - \ln S_{\max}(N/2)}{\ln N - \ln(N/2)}. \quad (19)$$

In the limit  $N \rightarrow \infty$ ,  $\psi_S = 1$  for  $\lambda < \lambda_{c2}$  and  $\psi_S = 0$  for  $\lambda > \lambda_{c2}$ , because the largest S-component size should be proportional to  $N$  for  $\lambda < \lambda_{c2}$  and finite for  $\lambda > \lambda_{c2}$ . As shown in Fig. 2(b), numerical results for  $\psi_S$  approach  $\psi_S = 1$  ( $\psi_S = 0$ ) for  $\lambda < \lambda_{c2}$  ( $\lambda > \lambda_{c2}$ ) as  $N$  increases, and have a crossing point at  $\lambda_{c2}$ . From numerical data, we have  $\psi_S^c \equiv \psi_S(\lambda_{c2}) = 2/3$  at  $\lambda_{c2} \simeq 0.615$ , which coincides well with our analytical estimate (the vertical line in Fig. 2).

This observation is also confirmed by a finite size scaling. As in [33], we assume a scaling form for  $S_{\max}(N)$  as

$$S_{\max}(\lambda, N) = N^{\psi_S^c} f_s[N(\Delta\lambda)^{\beta/(1-\psi_S^c)}], \quad (20)$$

where  $\Delta\lambda = |\lambda_{c2} - \lambda|$  and

$$f_s(x) \propto \begin{cases} \text{const} & \text{for } x \ll 1 \\ x^{1-\psi_S^c} & \text{for } x \gg 1 \end{cases}. \quad (21)$$

In Fig. 2(c), our scaling shows a nice collapse with  $\psi_S^c = 2/3$  and  $\beta = 1$ . These exponents mean that the percolation transition of the S-components actually occurs at  $\lambda_{c2}$  and belongs to the mean-field universality class.

## B. derivation of $\lambda_{c1}$

To derive  $\lambda_{c1}$  for the SIR model with multiple seeds, we need to calculate the connectivity of the R-components generated by each seed. We should note that a percolation analysis, as in the previous subsection, using the degree distribution of the R-components  $r_{\ell,0}/r$  is not applicable to this case, because such an analysis ignores the condition that *each R-component is connected*. To consider the connectivity of numerous R-components, we use the following procedure: (i) We first calculate the probability,  $P_n$ , that the size of the R-component generated by a single seed is  $n$ .

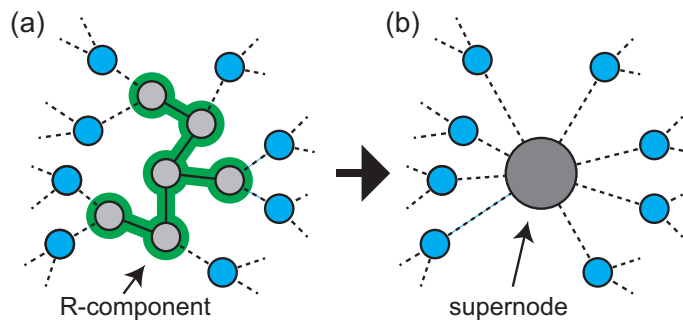


FIG. 3: Example of (a) an R-component and (b) the corresponding supernode. In this example, the R-component of size  $n = 6$  on a 3-RRG has  $n - 1 = 5$  edges inside (solid lines) and  $zn - 2(n - 1) = 8$  edges attaching to susceptible nodes (dashed lines). Then, the degree of the supernode is  $k_n = 8$ .

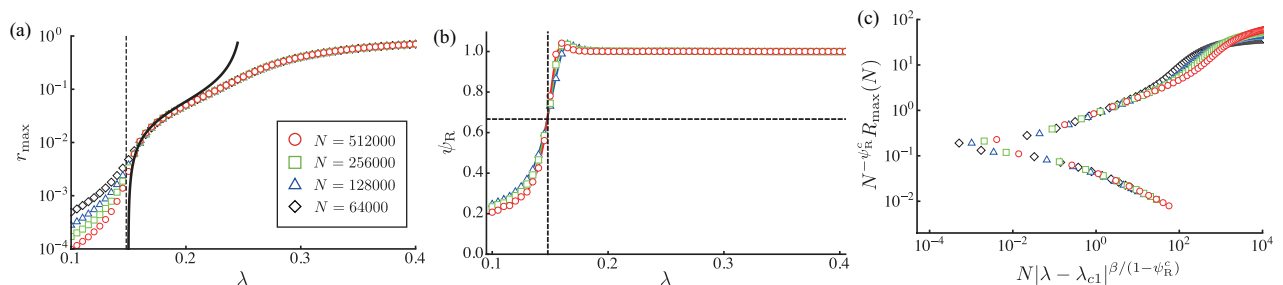


FIG. 4: (a) Fraction of the largest R-component  $r_{\max}$  as a function of  $\lambda$ . The points are obtained by Monte-Carlo simulations. The solid line is drawn by evaluating Eq.(C4). (b) Numerical results of the fractal exponent of the largest R-component,  $\psi_R$ . Data with several values of  $N$  have a crossing point at  $\lambda_{c1} = 0.148$  and  $\psi_R^c = 2/3$ . (c) Finite size scaling for  $R_{\max}$  around  $\lambda_{c1}$ . Here we set  $\psi_R^c = 2/3$  and  $\beta = 1$ , which means that the transition at  $\lambda_{c1}$  belongs to the mean-field universality class.

(ii) For the case of  $\rho > 0$ , the system has numerous R-components proportional to  $\rho$ . We regard each R-component as a supernode. The number of nodes confined in a supernode obeys the distribution  $P_n$ , and its degree  $k_n$  is given accordingly. (iii) Then, we consider a site percolation problem of supernodes. The first percolation point,  $\lambda_{c1}$ , is given as the critical point where the infinitely connected component of the supernodes appears.

In Appendix B, we evaluate the mean size of the R-component starting from a single seed,  $\langle n \rangle (= \sum_n P_n n)$ , and the corresponding mean square size,  $\langle n^2 \rangle (= \sum_n P_n n^2)$ , by using generating functions. Then, we consider the case of  $\rho > 0$ . Below  $\lambda_{c1}$ , we naturally assume that the mean size  $\langle n \rangle$  is so small that each R-component is a tree [40] and that any overlaps between the R-components are negligible so that the total fraction of the R-components can be evaluated as  $\rho \langle n \rangle$  [41], which should be necessarily less than 1. Then, we can determine the creation process of the infinite R-component by regarding each R-component with size  $n$  as a supernode whose degree depends on  $n$  (see Fig.3) and considering the percolation problem of these supernodes.

The density of susceptible nodes,  $s$ , is just one minus the density of the removed nodes,  $\rho \langle n \rangle$ :

$$s = 1 - \rho \langle n \rangle. \quad (22)$$

Then, the probability  $\tilde{p}$  that the node reached by following a randomly chosen link is a component of a supernode is

$$\tilde{p} = \frac{\rho \langle k_n \rangle}{\rho \langle k_n \rangle + zs}, \quad (23)$$

where  $k_n$  is the number of external links of the R-component (the degree of the supernode) having the size  $n$ , and is given by

$$k_n = (z - 2)n + 2. \quad (24)$$

Equation (24) holds since each R-component is a tree with the number of edges equal to the number of nodes minus one.



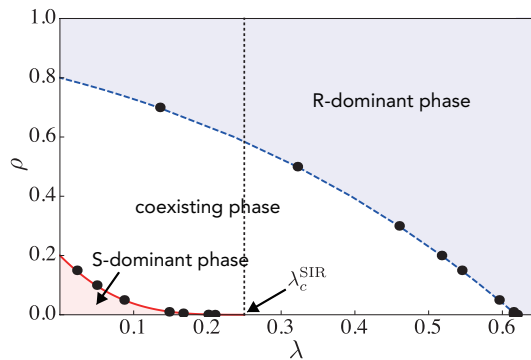


FIG. 5: Phase diagram in the  $(1 - \rho, \lambda)$ -space. The solid red and dashed blue lines are the analytically obtained  $\lambda_{c1}$  and  $\lambda_{c2}$ , respectively. The black circles are plotted by the crossings of  $\psi_R$  and  $\psi_S$ .

The mean branching ratio of supernodes,  $B$ , is evaluated by multiplying  $\tilde{p}$  by the mean excess degree of supernodes:

$$B = \tilde{p} \frac{\langle k_n(k_n - 1) \rangle}{\langle k_n \rangle} = \frac{\rho \langle k_n(k_n - 1) \rangle}{\rho \langle k_n \rangle + zs}. \quad (25)$$

The percolation of supernodes takes place when  $B \geq 1$ , and thus the transition point is given by  $B = 1$ . That is,  $\lambda_{c1}$  satisfies

$$\begin{aligned} \frac{z}{\rho} &= \langle k_n(k_n - 2) \rangle + z \langle n \rangle \\ &= z^2 \langle n^2 \rangle + (3z - 4) \langle n \rangle, \end{aligned} \quad (26)$$

where  $\langle n \rangle$  and  $\langle n^2 \rangle$  are functions of  $\lambda$ .

We can show that these moments diverge as  $\langle n \rangle \sim (\lambda_c^{\text{SIR}} - \lambda)^{-1}$  and  $\langle n^2 \rangle \sim (\lambda_c^{\text{SIR}} - \lambda)^{-3}$  when  $\lambda$  approaches  $\lambda_c^{\text{SIR}}$  from below (see Appendix B), and therefore  $\lambda_{c1} \rightarrow \lambda_c^{\text{SIR}}$  as  $\rho \rightarrow 0$  like

$$\lambda_c^{\text{SIR}} - \lambda_{c1} \sim \rho^{1/3}. \quad (27)$$

Thus, a small increase in  $\rho$  drastically reduces  $\lambda_{c1}$  from  $\lambda_c^{\text{SIR}}$ .

We approximately have the fraction of the largest R-component,  $r_{\text{max}}$ , by applying a similar procedure as the derivation of  $s_{\text{max}}$  to the connected components of supernodes (see Appendix C). This approximation may predict a rise of the order parameter  $r_{\text{max}}$  around  $\lambda_{c1}$ , but inherently overestimates  $r_{\text{max}}$  for  $\lambda > \lambda_{c1}$  due to the overlaps between the R-components generated from each seed being non-negligible (see Fig. 4 (a)).

We also check our estimate by comparing with Monte-Carlo simulations. In Figs. 4 (a) and (b), we plot the Monte-Carlo results for the order parameter,  $r_{\text{max}}(N)$ , and the corresponding fractal exponent,  $\psi_R(N) \equiv d \ln r_{\text{max}}(N) / d \ln N$ . In a similar manner to the previous subsection, we find that the crossing point of  $\psi_R$  is at our estimate of  $\lambda_{c1}$ . We also find a good scaling result for  $R_{\text{max}}(N)$  using  $\psi_R^c \equiv \psi_R(\lambda_{c1}) = 2/3$ ,  $\beta = 1$ , and obtained  $\lambda_{c1}$  (Fig. 4 (c)), supporting the validity of our estimate and indicating that the percolation transition at  $\lambda_{c1}$  belongs to the mean-field universality class.

### C. phase diagram

Finally, we analytically and numerically evaluate  $\lambda_{c1}$  and  $\lambda_{c2}$  for several values of  $\rho$ . In Fig. 5, we have the phase diagram of  $(\rho, \lambda)$ -space. We find that our estimates of  $\lambda_{c1}$  and  $\lambda_{c2}$  perfectly match with the Monte-Carlo results. The first percolation point  $\lambda_{c1}$  is smaller than  $\lambda_c^{\text{SIR}}$  as long as  $\rho > 0$ . That is, the percolation of the R-components occurs without global outbreaks. The gap between  $\lambda_{c1}$  and  $\lambda_c^{\text{SIR}}$  shrinks with decreasing  $\rho$  and  $\lambda_{c1} = \lambda_c^{\text{SIR}}$  in the limit  $\rho \rightarrow 0$ . Note that  $\lambda_{c1} = 0$  when  $\rho \geq 0.2$  because the seeds themselves percolate (the site percolation threshold of the  $z$ -regular RRG is  $1/(z - 1)$ ), and  $\lambda_{c2} = 0$  when  $\rho \geq 0.8$  because the seeds themselves disintegrate the susceptible network into finite components.

Our finite size scaling for several values of  $\rho$  shows that both percolation transitions at  $\lambda_{c1}$  and  $\lambda_{c2}$  belong to the mean-field universality class, irrespective of the value of  $\rho$ . This seems unsurprising because the two processes

comprising the present model, the SIR model and site percolation, belong to the mean-field universality class of percolation when the graph is RRG.

When  $\rho > 0$ , the system does not show any singular behavior at  $\lambda_c^{\text{SIR}}$ . However, this does not mean that  $\lambda_c^{\text{SIR}}$  is unimportant. In practice,  $\lambda_c^{\text{SIR}}$  is still an important measure in the strategy for disease control because a single seed has the potential to induce a global outbreak above  $\lambda_c^{\text{SIR}}$  (in other words, the basic reproduction number  $R_0 > 1$  when  $\lambda > \lambda_c^{\text{SIR}}$ ). The singular behaviors at  $\lambda_{c1}$ , e.g., the divergence of the R-susceptibility, may be interpreted as a precursor to global outbreaks, like a proverbial canary in a coal mine.

## V. SUMMARY

In this paper, we studied the SIR model on a RRG with a nontrivial fraction of infection seeds,  $\rho$ . Through analytical estimates and numerical simulations, we obtained the phase diagram in  $(\rho, \lambda)$ -space. The SIR model with numerous seeds shows the percolation transition of the removed and susceptible nodes at  $\lambda_{c1}$  and  $\lambda_{c2}$ , respectively. In particular,  $\lambda_{c1}$  is smaller than the epidemic threshold  $\lambda_c^{\text{SIR}}$  as long as  $\rho > 0$ . This means that epidemic clusters generated by multiple seeds percolate without global outbreaks.

So far, we have focused on the SIR model on the RRG. We expect that the above statement holds for the SIR model on other networks although the details of the phase transition may depend on network structures, e.g.,  $\lambda_{c1} < \lambda_c^{\text{SIR}} = 0$  on a fat-tailed scale-free network with  $\gamma \leq 3$ .

Finally, we briefly discuss other epidemic models with multiple seeds. Krapivsky et al. [34] proposed an extended SIR model, called a transient fad, with the assumption of a well-mixed population. They analytically showed that this model exhibits a discontinuous transition if  $\rho > 0$ . The authors and a collaborator [42] performed Monte-Carlo simulations for this fad model on networks to confirm that a discontinuous jump of the order parameter appears near the epidemic threshold, which is behind the percolation of epidemic clusters. The authors also investigated the discrete time version of the transient fad to confirm it numerically and analytically [35]. Very recently, several generalized epidemic models on networks beyond the classical SIR model have been investigated [36–39] It will be interesting to clarify what numerous seeds induce on such generalized epidemic models.

## Acknowledgements

TH's work was partially supported by the Grant-in-Aid for Young Scientists (B) (Grant No. 24740054 and No. 15K17716), Grant-in-Aid for Scientific Research (B) (Grant No. 26310203), and JST, ERATO, Kawarabayashi Large Graph Project.

### Appendix A: derivation of $\lambda_c^{\text{SIR}}$ for the limit $\rho \rightarrow 0$

The AMEs do not predict any transition point when  $\rho > 0$  because  $r > \rho > 0$ . However, it is possible to derive the transition point  $\lambda_c^{\text{SIR}}$  if the fraction of infection seeds is infinitesimally small ( $\rho \rightarrow 0$ ). In the AMEs for  $\{s_{t,m}\}$ , only  $s_{z,0}$  and  $s_{z-1,1}$  are relevant up to the first order of  $\rho$ :

$$\dot{s}_{z,0} = -\beta_s^{si} z s_{z,0}, \quad \dot{s}_{z-1,1} = -\lambda s_{z-1,1} + \beta_s^{si} z s_{z,0} - \beta_s^{ir} s_{z-1,1}, \quad (\text{A1})$$

with

$$\beta_s^{si} = \lambda \frac{(z-1)s_{z-1,1}}{z s_{z,0}}, \quad \beta_s^{ir} = \mu, \quad (\text{A2})$$

and the initial condition

$$s_{z,0}(0) = 1 - (z+1)\rho, \quad s_{z-1,1}(0) = z\rho. \quad (\text{A3})$$

Equation (A2) is substituted into Eq.(A1) to find the condition for  $s_{z-1,1}$  to remain finite as  $t \rightarrow \infty$ :

$$\frac{\mu}{\lambda} > z - 2, \quad (\text{A4})$$

and thus, the lower bound of  $\mu/\lambda$  gives the epidemic threshold,  $\lambda_c^{\text{SIR}} = \mu/(z-2)$ , which corresponds to the known result (1).



### Appendix B: distribution of the $r$ -component generated from a single seed

First, we evaluate the size distribution of the R-components created by a single seed. To do this, we need to know the probability,  $p_\ell^{(k)}$ , for an infected node to infect  $\ell$  out of  $k$  neighboring susceptible nodes before being removed. Such an infected node is removed before infecting any neighbors with a probability  $p_0^{(k)} = \frac{1}{1+k\lambda}$ , so that the probability of infecting at least one neighboring node before removal is  $1 - p_0^{(k)} = \frac{k\lambda}{1+k\lambda}$ . Since the infecting process is Markovian, we can express  $p_\ell^{(k)}$  as

$$p_\ell^{(k)} = \begin{cases} \frac{1}{1+k\lambda}, & \ell = 0, \\ \frac{k\lambda}{1+k\lambda} \times p_{\ell-1}^{(k-1)}, & 0 < \ell \leq k. \end{cases} \quad (\text{B1})$$

From this equation, we find that the generating function of  $p_\ell^{(k)}$ ,

$$g_k(x) = \sum_{\ell=0}^k p_\ell^{(k)} x^\ell, \quad (\text{B2})$$

satisfies the recursion relation

$$g_k(x) = \frac{1 + k\lambda x g_{k-1}(x)}{1 + k\lambda} \quad (\text{B3})$$

with  $g_0(x) = 1$ .

Now, let  $P_n$  be the probability that a single seed creates an R-component of size  $n$ , and let  $Q_n$  be the probability that a node infected by another node further creates a partial R-component of size  $n$ . Then, by considering the infection process starting from a single seed,  $P_n$  can be evaluated as

$$P_n = \sum_{\ell=0}^z p_\ell^{(z)} \sum_{m_1, m_2, \dots, m_\ell} Q_{m_1} Q_{m_2} \cdots Q_{m_\ell} \delta_{n, 1 + \sum_{\mu=0}^{\ell} m_\mu}. \quad (\text{B4})$$

Similarly,  $Q_n$  can be recursively given as

$$Q_n = \sum_{\ell=0}^{z_1} p_\ell^{(z_1)} \sum_{m_1, m_2, \dots, m_\ell} Q_{m_1} Q_{m_2} \cdots Q_{m_\ell} \delta_{n, 1 + \sum_{\mu=0}^{\ell} m_\mu}, \quad (\text{B5})$$

where  $z_\nu = z - \nu$ . Introducing the corresponding generating functions,

$$G_0(x) = \sum_{n=1}^{\infty} P_n x^n, \quad G_1(x) = \sum_{n=1}^{\infty} Q_n x^n, \quad (\text{B6})$$

we can express the above relations (B4) and (B5) in a compact form as

$$G_0(x) = x g_z(G_1(x)) \quad (\text{B7})$$

and

$$G_1(x) = x g_{z_1}(G_1(x)), \quad (\text{B8})$$

respectively.

What we want to know is the mean size of the R-component,  $\langle n \rangle = G'_0(1)$ , and the mean square size of the R-component,  $\langle n^2 \rangle = G''_0(1) + G'_0(1)$ . To evaluate these values, we need the derivative of  $g_k(x)$ , which is given by

$$g'_k(x) = \frac{k\lambda}{1+k\lambda} [g_{k-1}(x) + x g'_{k-1}(x)], \quad (\text{B9})$$

from which the mean value  $\langle \ell \rangle_k$  can be easily found to be

$$\langle \ell \rangle_k = g'_k(1) = \frac{k\lambda}{1+\lambda}. \quad (\text{B10})$$

One also requires the second derivative:

$$g_k''(x) = \frac{k\lambda}{1+k\lambda} [2g_{k-1}'(x) + xg_{k-1}''(x)], \quad (\text{B11})$$

so that

$$\langle \ell(\ell-1) \rangle_k = g_k''(1) = \frac{2k(k-1)\lambda^2}{(1+\lambda)(1+2\lambda)}, \quad (\text{B12})$$

yielding

$$\langle \delta\ell^2 \rangle_k = \langle \ell^2 \rangle_k - \langle \ell \rangle_k^2 = \frac{k\lambda[1+(k+1)\lambda]}{(1+\lambda)^2(1+2\lambda)}. \quad (\text{B13})$$

Now we can evaluate the derivatives of  $G_0(x)$  as

$$G_0' = g_z(G_1) + xg_z'(G_1)G_1', \quad (\text{B14})$$

$$G_0'' = 2g_z'(G_1)G_1' + xg_z''(G_1)G_1'^2 + xg_z'(G_1)G_1'', \quad (\text{B15})$$

and

$$G_1' = g_{z_1}(G_1) + xg_{z_1}'(G_1)G_1', \quad (\text{B16})$$

$$G_1'' = 2g_{z_1}'(G_1)G_1' + xg_{z_1}''(G_1)G_1'^2 + xg_{z_1}'(G_1)G_1''. \quad (\text{B17})$$

Setting  $x = 1$  gives  $G_1(1) = 1$  and

$$G_1'(1) = 1 + g_{z_1}'(1)G_1'(1) = \frac{1}{1-g_{z_1}'(1)} = \frac{1}{1-\langle \ell \rangle_{z_1}}, \quad (\text{B18})$$

$$\begin{aligned} G_1''(1) &= 2g_{z_1}'(1)G_1'(1) + g_{z_1}''(1)G_1'(1)^2 + g_{z_1}'(1)G_1''(1) \\ &= G_1'(1)^3 [2g_{z_1}'(1)(1-g_{z_1}'(1)) + g_{z_1}''(1)]. \end{aligned} \quad (\text{B19})$$

These quantities provide an explicit expression for the first moment,  $M_1$ , and the second cumulant,  $C_2$  (and thus the second moment  $M_2 = C_2 + M_1^2$ ) of  $P_n$  as

$$M_1 = \langle n \rangle = G_0'(1) = 1 + \langle \ell \rangle_z G_1'(1), \quad (\text{B20})$$

$$\begin{aligned} C_2 &= \langle n^2 \rangle - \langle n \rangle^2 \\ &= G_0''(1) + M_1 - M_1^2 \\ &= G_1'(1)^2 [g_z''(1) + g_z'(1) - g_z'(1)^2] + g_z'(1) [G_1''(1) + G_1'(1) - G_1'(1)^2] \\ &= G_1'(1)^2 \langle \delta\ell^2 \rangle_z + G_1'(1)^3 \langle \ell \rangle_z \langle \delta\ell^2 \rangle_{z_1}. \end{aligned} \quad (\text{B21})$$

When  $\lambda$  approaches  $\lambda_c^{\text{SIR}}$  from below,  $G_1'(1)$  dominates the behavior of  $M_1$  and  $C_2$ . Indeed (B18) tells us that  $G_1'(1)$  diverges as  $\delta\lambda^{-1}$ , where  $\delta\lambda = \lambda_c^{\text{SIR}} - \lambda$ , and thus

$$M_1 = \langle n \rangle \sim \delta\lambda^{-1}, \quad C_2 \sim \langle n^2 \rangle \sim \delta\lambda^{-3}. \quad (\text{B22})$$

### Appendix C: largest R-component size

The generating function of the probability for a supernode to have the degree  $k_n$  is given by

$$H_0(x) = \sum_{n=1}^{\infty} P_n x^{k_n} = x^2 G_0(x^{z_2}), \quad (\text{C1})$$

and that of the excess degree as

$$H_1(x) = \frac{H'_0(x)}{H'_0(1)} = \frac{2xG_0(x^{z_2}) + z_2x^{z_1}G'_0(x^{z_2})}{\langle k_s \rangle}. \quad (\text{C2})$$

Let  $u$  be the probability that a finite cluster of supernodes is found by following randomly chosen links; this satisfies

$$u = 1 - \tilde{p} + \tilde{p}H_1(u). \quad (\text{C3})$$

Then, the density of the largest component of supernodes in size, i.e.,  $r_{\max}$ , is evaluated as

$$r_{\max} = \rho \sum_{n=1}^{\infty} nP_n(1 - u^{k_n}) = \rho[\langle n \rangle - u^z G'_0(u^{z_2})]. \quad (\text{C4})$$

- [1] W. O. Kermack and A. G. McKendrick, in *Proceedings of the Royal Society of London A: Mathematical, Physical and Engineering Sciences* (The Royal Society, 1927), vol. 115, pp. 700–721.
- [2] R. M. Anderson and R. M. May, *Infectious Diseases of Humans: Dynamics and Control* (Oxford University press, 1992).
- [3] R. Pastor-Satorras, C. Castellano, P. Van Mieghem, and A. Vespignani, *Reviews of Modern Physics* **87**, 925 (2015).
- [4] R. Albert and A.-L. Barabási, *Rev. Mod. Phys.* **74**, 47 (2002).
- [5] M. E. J. Newman, *SIAM review* **45**, 167 (2003).
- [6] S. N. Dorogovtsev, A. V. Goltsev, and J. F. F. Mendes, *Rev. Mod. Phys.* **80**, 1275 (2008).
- [7] A. Barrat, M. Barthélemy, and A. Vespignani, *Dynamical processes on complex networks* (Cambridge University Press, Cambridge, 2008).
- [8] Y. Moreno, R. Pastor-Satorras, and A. Vespignani, *The European Physical Journal B-Condensed Matter and Complex Systems* **26**, 521 (2002).
- [9] P. Grassberger, *Mathematical Biosciences* **63**, 157 (1983).
- [10] M. E. J. Newman, *Physical Review E* **66**, 016128 (2002).
- [11] J. C. Miller, A. C. Slim, and E. M. Volz, *Journal of the Royal Society Interface* **9**, 890 (2012).
- [12] J. Lindquist, J. Ma, P. Van den Driessche, and F. H. Willeboordse, *Journal of Mathematical Biology* **62**, 143 (2011).
- [13] J. P. Gleeson, *Physical Review Letters* **107**, 068701 (2011).
- [14] J. P. Gleeson, *Physical Review X* **3**, 021004 (2013).
- [15] R. Pastor-Satorras and A. Vespignani, *Physical Review E* **65**, 036104 (2002).
- [16] N. Madar, T. Kalisky, R. Cohen, D. ben-Avraham, and S. Havlin, *The European Physical Journal B-Condensed Matter and Complex Systems* **38**, 269 (2004).
- [17] L. K. Gallos, F. Liljeros, P. Argyrakis, A. Bunde, and S. Havlin, *Physical Review E* **75**, 045104 (2007).
- [18] R. Cohen, S. Havlin, and D. ben-Avraham, *Physical Review Letters* **91**, 247901 (2003).
- [19] P. Holme, *EPL* **68**, 908 (2004).
- [20] Y. Chen, G. Paul, S. Havlin, F. Liljeros, and H. E. Stanley, *Physical Review Letters* **101**, 058701 (2008).
- [21] J. C. Miller, *PLoS ONE* **9**, e101421 (2014).
- [22] Z.-L. Hu, J.-G. Liu, G.-Y. Yang, and Z.-M. Ren, *EPL* **106**, 18002 (2014).
- [23] S. Ji, L. Lu, C. H. Yeung, and Y. Hu, *arXiv preprint arXiv:1508.04294* (2015).
- [24] E. Kenah and J. C. Miller, *Interdisciplinary Perspectives on Infectious Diseases* **2011** (2011).
- [25] T. Tomé and R. M. Ziff, *Physical Review E* **82**, 051921 (2010).
- [26] D. R. de Souza, T. Tomé, and R. M. Ziff, *Journal of Statistical Mechanics: Theory and Experiment* **2011**, P03006 (2011).
- [27] M. E. J. Newman, *Physical Review Letters* **95**, 108701 (2005).
- [28] M. J. Ferrari, S. Bansal, L. A. Meyers, and O. N. Bjørnstad, *Proceedings of the Royal Society of London B: Biological Sciences* **273**, 2743 (2006).
- [29] S. Bansal and L. A. Meyers, *Journal of Theoretical Biology* **309**, 176 (2012).
- [30] L. D. Valdez, P. A. Macri, and L. A. Braunstein, *Physical Review E* **85**, 036108 (2012).
- [31] T. Hasegawa and N. Masuda, *Journal of Statistical Mechanics: Theory and Experiment* **2011**, P09014 (2011).
- [32] T. Hasegawa, K. Konno, and K. Nemoto, *The European Physical Journal B* **85**, 1 (2012).
- [33] T. Hasegawa, T. Nogawa, and K. Nemoto, *EPL* **104**, 16006 (2013).
- [34] P. L. Krapivsky, S. Redner, and D. Volovik, *Journal of Statistical Mechanics: Theory and Experiment* **2011**, P12003 (2011).
- [35] T. Hasegawa and K. Nemoto, *Journal of Statistical Mechanics: Theory and Experiment* **2014**, P11024 (2014).
- [36] G. Bizhani, M. Paczuski, and P. Grassberger, *Physical Review E* **86**, 011128 (2012).
- [37] K. Chung, Y. Baek, D. Kim, M. Ha, and H. Jeong, *Physical Review E* **89**, 052811 (2014).
- [38] W. Cai, L. Chen, F. Ghanbarnejad, and P. Grassberger, *Nature physics* (2015).
- [39] J. Gómez-Gardeñes, A. S. de Barros, S. T. Pinho, and R. F. Andrade, *EPL* **110**, 58006 (2015).
- [40] Finite components have no cyclic path in infinite locally tree-like networks.

- [41] This condition means that the total size of the R-components is smaller than the number of nodes. Let us consider a finite network with  $N$  nodes. The number of seeds is  $N\rho$ , and the mean R-component size for each seed is  $\langle n \rangle$ . Then total size of the R-components is  $N\rho\langle n \rangle$ . Our assumption is equivalent that  $N\rho\langle n \rangle < N$ .
- [42] T. Hasegawa, N. Kinoshita, and K. Nemoto, in preparation.